available at www.sciencedirect.com
journal homepage: www.eu-openscience.europeanurology.com

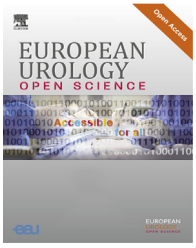

European Association of Urology

Prostate Cancer

Side-specific, Microultrasound-based Nomogram for the Prediction of Extracapsular Extension in Prostate Cancer

Adriana M. Pedraza [a,*], *Sneha Parekh* [a], *Himanshu Joshi* [a,b], *Ralph Grauer* [a], *Vinayak Wagaskar* [a], *Laura Zuluaga* [a], *Raghav Gupta* [a], *Flora Barthe* [a], *Jordan Nasri* [a], *Krunal Pandav* [a], *Dhruti Patel* [a], *Michael A. Gorin* [a], *Mani Menon* [a], *Ashutosh K. Tewari* [a,*]

[a] *Department of Urology, Icahn School of Medicine at Mount Sinai, New York City, NY, USA;* [b] *Institute for Healthcare Delivery Science, Department of Population Health Science and Policy, Icahn School of Medicine at Mount Sinai, New York, NY, USA*

Article info

Article history:
Accepted December 1, 2022

Associate Editor:
Guillaume Ploussard

Keywords:
Prostate cancer
Extracapsular extension
Microultrasound
Multiparametric magnetic resonance imaging

Abstract

Background: Prediction of extracapsular extension (ECE) is essential to achieve a balance between oncologic resection and neural tissue preservation. Microultrasound (MUS) is an attractive alternative to multiparametric magnetic resonance imaging (mpMRI) in the staging scenario.
Objective: To create a side-specific nomogram integrating clinicopathologic parameters and MUS findings to predict ipsilateral ECE and guide nerve sparing.
Design, setting, and participants: Prospective data were collected from consecutive patients who underwent robotic-assisted radical prostatectomy from June 2021 to May 2022 and had preoperative MUS and mpMRI. A total of 391 patients and 612 lobes were included in the analysis.
Outcome measurements and statistical analysis: ECE on surgical pathology was the primary outcome. Multivariate regression analyses were carried out to identify predictors for ECE. The resultant multivariable model's performance was visualized using the receiver-operating characteristic curve. A nomogram was developed based on the coefficients of the logit function for the MUS-based model. A decision curve analysis (DCA) was performed to assess clinical utility.
Results and limitations: The areas under the receiver-operating characteristic curve (AUCs) of the MUS-based model were 81.4% and 80.9% (95% confidence interval [CI] 75.6, 84.6) after internal validation. The AUC of the mpMRI-model was also 80.9% (95% CI 77.2, 85.7). The DCA demonstrated the net clinical benefit of the MUS-based nomogram and its superiority compared with MUS and MRI alone for detecting ECE. Limitations of our study included its sample size and moderate inter-reader agreement.
Conclusions: We developed a side-specific nomogram to predict ECE based on clinicopathologic variables and MUS findings. Its performance was comparable with

* Corresponding authors at: Department of Urology, Icahn School of Medicine at Mount Sinai, New York City, NY 10029, USA. Tel. +1 2122416500.
E-mail addresses: adriana.pedrazabermeo@mountsinai.org (A.M. Pedraza), ash.tewari@mountsinai.org (A.K. Tewari).

https://doi.org/10.1016/j.euros.2022.12.005

that of a mpMRI-based model. External validation and prospective trials are required to corroborate our results.

Patient summary: The integration of clinical parameters and microultrasound can predict extracapsular extension with similar results to models based on magnetic resonance imaging findings. This can be useful for tailoring the preservation of nerves during surgery.

1. Introduction

The preoperative detection of extracapsular extension (ECE) guides the surgical plane of dissection, dictating the grade of nerve sparing to be performed [1–3]. A balance between preservation of the "neural hammock" and a fuller prostatic fascial resection affects key outcomes, including surgical margin status, urinary continence, and erectile function [4–8]. Consequently, extensive research has been conducted to optimize preoperative ECE prediction.

American Urological Association states that multiparametric magnetic resonance imaging (mpMRI) should not be used in isolation to determine nerve sparing as its ability to predict ECE, particularly when microscopic, is suboptimal [9]. Moreover, the European guideline recommends not performing nerve-sparing surgery on patients classified to have >T2c or International Society of Urological Pathology (ISUP) Gleason grading group (GGG) >3 [10]. Given the growing preoperative use of mpMRI, several authors have explored the additive value of this technology to clinical variables in the prediction of ECE, and although multiple models have been described, most of them lack external validation [11–14]. Besides, limitations of mpMRI include its low sensitivity, low negative predictive value (NPV) for ECE detection, long learning curve, cost, and moderate inter-reader reproducibility [10,15,16].

An emerging technology that offers promise as a possible adjunct and alternative to mpMRI is high-definition microultrasound (MUS). MUS functions via a transrectal probe that operates at 29 MHz, as opposed to 8–12 MHz with traditional ultrasound systems to provide resolution down to 70 μm, a 300% improvement over current standards [17]. Meta-analysis evidence supports equivalence between MUS- and mpMRI-targeted biopsies in detecting clinically significant prostate cancer [18]. In addition, MUS provides a real-time anatomic assessment, has lower cost and no-lag acquisition time, avoids intravenous contrast, and has fewer contraindications than MRI, and the fundamentals of its use are the same as traditional ultrasound—a modality that many urologists are familiar with. Although the exact role of MUS has yet to be established in guideline recommendations, the potential is clear.

The extent of neural hammock preservation is influenced greatly by imaging findings. In a recent meta-analysis, mpMRI modified the surgical plan in 35% of the cases, showing an accurate decision in 77% of them. This accuracy increased to 91% in high-risk prostate cancer patients [19]. Similarly, MUS could lead to achieving a better balance between nerve preservation and oncologic resection. To test this hypothesis, however, further research is required.

Given its promising outcomes in the detection of prostate cancer as well as local staging [18,20,21], we aimed to create a side-specific nomogram integrating clinicopathologic parameters and MUS findings to predict ipsilateral ECE.

2. Patients and methods

2.1. Study population

We included prospective data from 391 consecutive patients who had preoperative MUS and mpMRI and underwent robotic-assisted radical prostatectomy (RARP) from June 2021 to May 2022. Patients unable or unwilling to undergo mpMRI and MUS, and those who had received prior local (radiotherapy or focal therapy) or systemic therapy (androgen deprivation) were excluded.

The grading system described by Tewari et al [5] served as the foundation of our nerve-sparing technique. The extent of neural hammock preservation was tailored in a side-specific manner taking into account the ipsilateral risk of ECE according to Martini et al's [11] nomogram.

This study was covered under the institutional review board (STUDY-14-00050-CR002). As part of the protocol, all patients had a standard systematic (12-core) transrectal biopsy plus two to four cores from targeted areas in cases of mpMRI Prostate Imaging Reporting and Data System (PI-RADS) $\geq$3. All external biopsy slides were re-read in our center by an experienced pathologist, and all the surgeries were performed by a single surgeon (A.K.T.).

2.2. Outcome

The presence of ECE in final surgical pathology was the primary outcome. According to the ISUP, ECE was defined as the presence of a tumor beyond the borders of the gland; both ECE and seminal vesicle invasion were included in the analysis. Moreover, quantification of ECE was performed following the Epstein approach and reported as focal or established [22]. Since the goal of our study was to create a side-specific nomogram, prostate lobes with positive biopsy results were evaluated separately. A total of 391 patients and 612 lobes were included in the final analysis.

The protocol at our institution follows the ISUP Consensus guidelines on prostatectomy handling, and processing [23]. After specimen fixation and capsular inking for orientation, the apex is removed perpendicularly and the prostate's right and left posterior-lateral aspects. The base is taken en face and is sectioned perpendicularly. Then, the specimen is serially sectioned transversely from the apex to the base, and representative sections are submitted sequentially.

2.3. Imaging and interpretation

Patients underwent transrectal MUS 1–2 wk before surgery using the ExactVu system (Exact Imaging, Markham, Canada). This transrectal ultrasound was performed by an experienced urologist (A.M.P.) blinded

to mpMRI and biopsy results. The same urologist classified the lesions according to the Prostate Risk Identification Using Micro-Ultrasound (PRI-MUS) score. The dominant lesion on MUS was defined as the lesion with the highest PRI-MUS score or the largest in the case of multiple lesions with the same PRI-MUS score. Patients underwent 3-Tesla MRI with a pelvic phased-array coil before (363/391) or at least 4 wk after prostate biopsy (28/391). Of note, at our facility, targeted samples were guided by mpMRI (PI-RADS 3,4,5), whereas MUS technology was not used at the time of the biopsy.

Irrespective of the institution where mpMRI was performed, all images were uploaded to our Picture Archiving and Communication System (PACS; Centricity; GE Healthcare, Chicago, IL, USA). The mpMRI scans performed at our institution were read by dedicated radiologists and followed the technical specifications determined by the American College of Radiology, using 3-Tesla MRI systems (Magnetom Skyra; Siemens Healthineers, Erlangen, Germany, and Discovery MR750; GE Healthcare) equipped with either a 32- or an 18-element phased-array pelvic coil. Multiplanar T1-, T2-, and diffusion-weighted sequences were obtained, including axial T1 perfusion before and after contrast injection. PI-RADS version 2.1 was used [24].

A random sample of 78 patients—20% of the cohort—was selected for inter-reader agreement analyses. Three additional readers, a diagnostic medical sonographer (reader 2) and two urologists (readers 3 and 4), retrospectively reviewed and interpreted still images. Reader 2 had performed an average of 800 MUS scans, while readers 3 and 4 had performed an average of 500 and 400 MUS scans, respectively.

2.4. Variables and definitions

Prostate-specific antigen density (PSAD), maximum percentage of tumor involvement in the core with the highest Gleason score, ISUP grade group at biopsy, and ECE detected by imaging (MUS or mpMRI) were included in our model. Following PI-RADS v2.1, the asymmetry or invasion of the neurovascular bundles, bulging prostatic contour, irregular or spiculated margin, obliteration of the rectoprostatic angle, tumor-capsule interface of >1.0 cm, and breach of the capsule with evidence of direct tumor extension or bladder wall invasion were taken as signs of ECE presence on mpMRI [24]. Similarly, MRI-derived parameters were used for MUS, as described previously in the literature. These features specifically included capsular contact length $\geq$15 mm, capsular bulging or irregularity, visible breach of the prostate capsule, presence of a hypoechoic halo—mainly on apical lesions, and obliteration of the prostatic-seminal vesicle angle (Fig. 1) [20,21].

2.5. Statistical analysis

Baseline descriptive characteristics of the cohort were summarized as median and interquartile range for continuous variables. Categorical variables were summarized as frequency and percentages. The distribution of descriptive covariates by ECE status was compared for corresponding prostate specimen sides using chi-square for categorical variables and a *t* test for continuous variables.

Since we sought to compare the performance of the MRI- and MUS-based models, we developed two models using logistic regression: one based on MUS-based predictors and the other based on MRI-based predictor variables. After performing univariate binary logistic regression analyses, variables identified to be significantly associated with ipsilateral ECE ($p < 0.05$) were included in a multivariable binary logistic regression analysis to identify the predictors of ECE. The goodness of fit was assessed by using the likelihood ratio test ($p < 0.05$). The resultant multivariable model's performance was visualized using the receiver-operating characteristic (ROC) curve. The area under the ROC curve (AUC) was estimated. A nomogram was developed based on the coefficients of the logit function for the MUS-based model, and a decision curve analysis (DCA) was performed to assess the utility of our model. Lastly, *k*-fold cross-validation for the AUC for a binary outcome was performed after fitting a logit regression model, averaging the AUCs corresponding to each fold, and bootstrapping the cross-validated AUC to obtain statistical inference and 95% confidence intervals (CIs) [25].

To determine the additive value of combining mpMRI, MUS, and clinical parameters, we used the multilayer perceptron network models with backpropagation. The dataset was divided randomly into two sets: 69.6% (426) of the cases were used for training and 30.4% (186) for testing the model. Three layers were used in the neural network analysis (NNA): An input layer, a hidden layer, and an output layer. Nine covariates were included in the input layer—ISUP GGG, maximum percentage of core involvement in the core with the highest GGG, presence or absence of ECE on MUS and MRI, PSAD based on MRI volume, PSAD based on MUS volume, digital rectal examination (DRE), and PRI-MUS and PI-RADS scores. We applied the sigmoid activation function in the hidden layer and the softmax function in the output layer.

To assess the inter-reader agreement between MUS readers, the method described by Gwet [26] in 2014 was applied [27], and the classification proposed by Landis and Koch [28] was used to determine the levels of agreement: slight (0–0.20), fair (0.21–0.40), moderate (0.41–0.60), substantial (0.61–0.80), and excellent (0.81–1). Statistical analyses were carried out using STATA 14 (StataCorp, College Station, TX, USA). The NNA was performed with IMB SPSS, version 28.0.1.1 (SPSS Inc., Chicago, IL, USA).

3. Results

3.1. Population characteristics

The baseline characteristics are presented in Tables 1 and 2. In Summary, of the 612 prostatic lobes analyzed on the final pathology, 476 (78%) had organ-confined disease (OCD), while ECE was detected in 136 (22%). Age distribution, DRE, ISUP grade group, prostate-specific antigen (PSA), PSAD, PRI-MUS score, and PI-RADS score were significantly different among patients with OCD and those with ECE. The sensitivity, specificity, positive predictive value (PPV), and NPV of MUS for detecting ECE were 47.6%, 85.8%, 51.5%, and 83.8%, respectively. Comparatively, these parameters for mpMRI were 50%, 86.9%, 52.3%, and 85.9%, respectively. Of note, 41% of pT3a cases in final pathology had a focal extension, 12% presented with bladder neck invasion, and 47% had established ECE. Overall, ECE was present on the left side in 52 (38%) lobes, while 58 (43%) cases were documented on the right side, and 26 prostates (19%) presented with bilateral lobe involvement. Regarding surgical margin status, 45 (11.5%) patients were found to have positive margins. Of these, 19 (42%) had pT2 disease, and 26 (58%) had pT3a or pT3b disease.

3.2. Uni- and multivariable analyses predicting ECE

Univariate analysis results are presented in Table 3. The PSA level, PSAD, DRE, maximum percentage of tumor involvement in the core with the highest Gleason score, presence of ECE on MUS and mpMRI, PI-RADS 4 and 5, PRI-MUS scores 4 and 5, and ISUP GGG 4 and 5 were found to be statistically significant predictors of ECE.

On a multivariable analysis, two different models were assessed. The first model integrated MUS-based findings

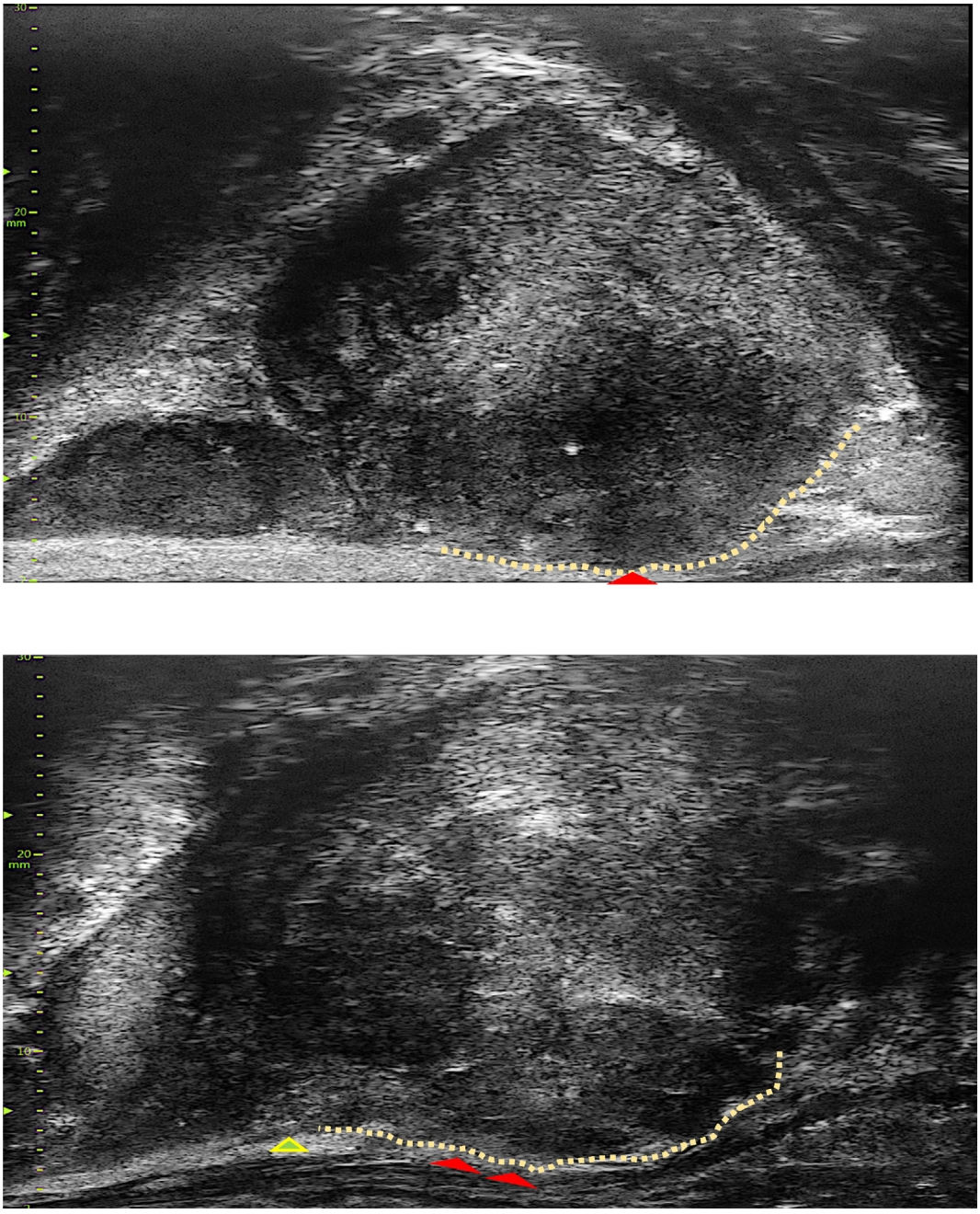

Fig. 1 – Examples of MRI-derived parameters to detect ECE with MUS: capsular contact length ≥15 mm, capsular bulging and irregularity (yellow dotted line), visible breach of the prostate (red arrow), and obliteration of the prostatic-seminal vesicle angle (green arrow). ECE = extracapsular extension; MRI = magnetic resonance imaging; MUS = microultrasound.

and clinical parameters. The PSAD, ISUP GGG, maximum percentage of core involvement in the core with the highest GGG, and presence of ECE on MUS emerged as significant predictors. These four prognostic indicators were used to construct the nomogram presented in Figure 2. The second model combined PSAD, ISUP GGG, maximum percentage of core involvement in the core with the highest GGG, and detection of ECE on mpMRI (Tables 3 and 4).

The AUC of the MUS- and MRI-based models were 81.4% and 82%, respectively. Following internal validation, both models presented with excellent performance with an AUC of 80.9% (MUS: 95% CI 75.6, 84.6; mpMRI: 95% CI 77.2, 85.7). The DCA shown in Figure 3 demonstrates the net clinical benefit of using the MUS-based nomogram and its superiority compared with MUS or MRI alone for the detection of ECE. Moreover, the test for equality of the AUCs comparing our model versus clinicopathologic parameters only (ie, without MUS) showed a statistically significant difference in favor of adding MUS as a predictor ($p = 0.014$).

A binary logistic regression was carried out to determine the performance of MUS (alone) according to the location of the ECE (base, mid prostate, apex, or anterior/posterior zones), followed by a test for the equality of AUCs. The

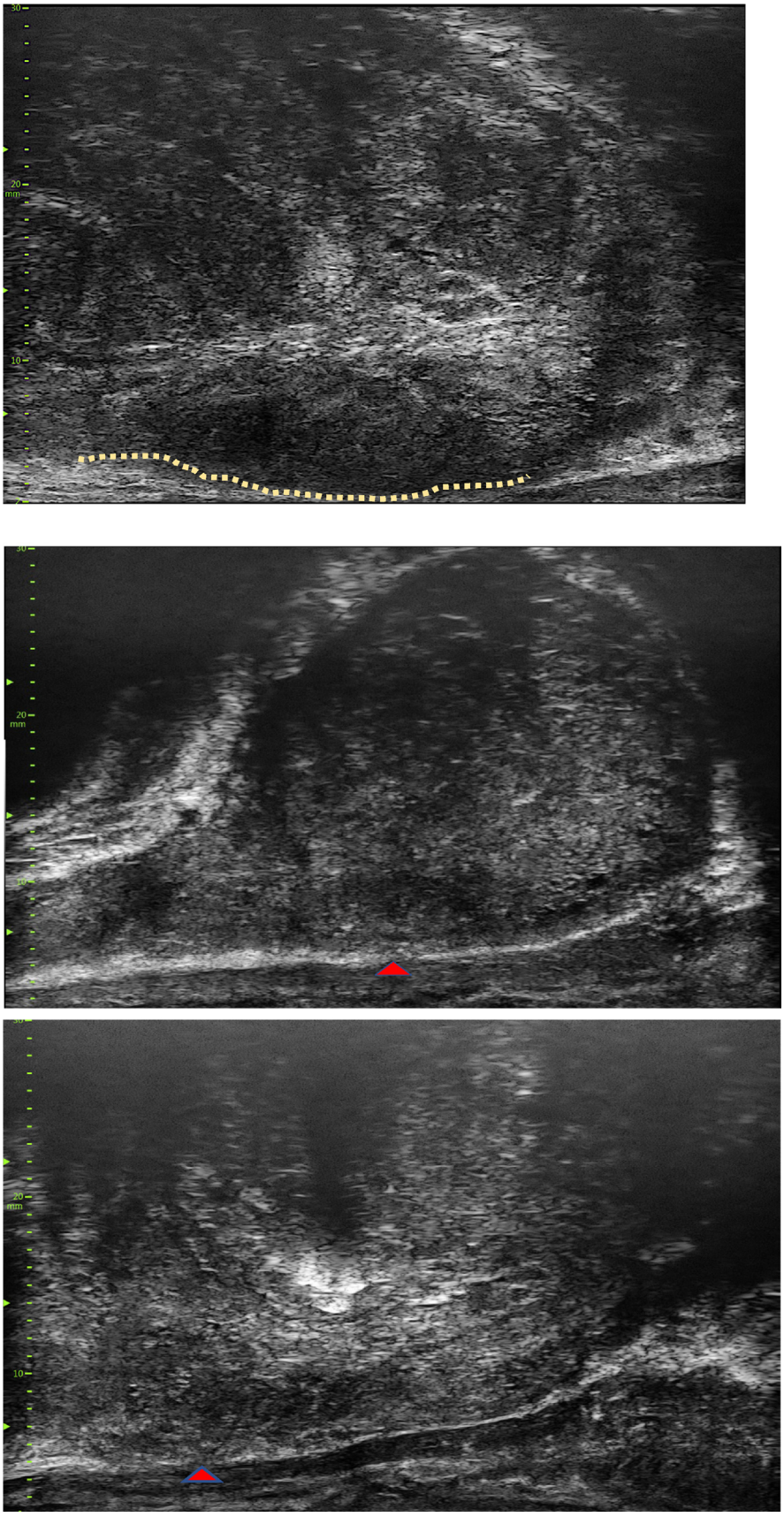

Fig. 1 (*continued*)

Table 1 – Descriptive characteristics of 391 patients who underwent robot-assisted radical prostatectomy at a single center between June 2021 and May 2022

Variable	Overall (n = 391)
Age at surgery (yr), median (IQR)	64 (59–69)
Preoperative PSA (ng/ml), median (IQR)	6.6 (4.8–9.8)
Family history, n (%)	119 (30)
Race, n (%)	
Caucasian	261 (67)
African American	70 (18)
Other	60 (15)
Clinical stage, n (%)	
T1c	277 (71)
T2	106 (27)
T3	8 (2)
Biopsy ISUP grade group, n (%)	
1	35 (9)
2	170 (43.5)
3	99 (25.3)
4	53 (13.5)
5	34 (8.7)
Maximum % core involvement, median (IQR)	50 (24–75)
Pathologic stage, n (%)	
T2	277 (70.8)
T3a	75 (19.2)
T3b	39 (10)
Pathologic ISUP grade group, n (%)	
1	20 (5.1)
2	231(59.0)
3	100 (25.6)
4	11(2.8)
5	29 (7.5)
NeuroSAFE status, n (%)	
Negative	287 (73.4)
Positive	104 (26.6)
Surgical margin status, n (%)	
Negative	346 (88.5)
Positive	45 (11.5)

IQR = interquartile range; ISUP = International Society of Urological Pathology; PSA = prostate-specific antigen.

MUS tented to perform better in the detection of ECE located at the apex (AUC 71%) and the posterior zone (AUC 69.1%) than that at the anterior (AUC 63%) and the base to midprostate (AUC 67.3%) zones. Nonetheless, these differences were not statistically significant (Supplementary Table 2). Of note, the agreement coefficient (AC) on ECE detection at MUS was fair among the four readers. However, the percentage of agreement between more experienced readers (1 and 2) was higher (73%) with a moderate AC (0.53, 95% CI 0.33–0.73; Table 5).

Lastly, the NNA, which included nine covariates of clinical significance, achieved the highest performance in detecting ECE with an AUC of 83.6%. Notably, the PSAD (prostatic volume by MUS) was the most critical contributor to the model (100%), followed by the maximum percentage of core involvement in the core with the highest GGG (93.9%), PSAD (prostatic volume by mpMRI; 52.8%), presence of ECE on MUS (45%), ISUP GGG (36.7%), presence of ECE on mpMRI (31%), PRI-MUS (25.9%), PI-RADS (24.3%), and DRE (12.1%; Supplementary Tables 1 and 2).

4. Discussion

An accurate assessment of ECE risk is of great importance as it will guide the surgeon in achieving an appropriate balance between oncologic resection and preservation of the "neural hammock." Since the creation of Partin tables to predict final pathology on radical prostatectomy, prognostic models have been expanded beyond the original use of PSA, Gleason score, and clinical stage to include an assortment of preoperative clinicopathologic and imaging-based variables, mainly mpMRI [29,30]. Although this technology has become a fundamental instrument in preoperative planning, sensitivity in the staging setting is still limited. Furthermore, few models provide a side-specific risk of ECE to inform the ipsilateral degree of nerve sparing [11,31–33].

We used a multivariate binary logistic regression to develop the first MUS-based nomogram to predict ipsilateral ECE on surgical pathology from a combination of MUS

Table 2 – Descriptive characteristics of 612 prostate specimen sides

Variable	Overall, N = 612	OCD N = 476 (78%)	ECE N = 136 (22%)	p value
Age at surgery (yr), median (IQR)	63 (59–69)	63.5 (58.0, 69.0)	65.0 (62.0, 71.5)	0.007
Preoperative PSA (ng/ml), median (IQR)	9.04 (4.8–9.9)	7.7 (4.7, 9.2)	13.6 (5.2, 13.0)	<0.0001
Abnormal DRE, n (%)	116	64 (13)	52 (38)	<0.0001
PSAD (MRI volume), median (IQR)	0.28 (0.13–0.33)	0.23 (0.14–0.30)	0.46 (0.18–0.49)	<0.0001
PSAD (MUS volume), median (IQR)	0.23 (0.11–0.28)	0.20 (0.10–0.25)	0.37 (0.14–0.42)	<0.0001
PI-RADS (%)				
2	161 (26)	146 (30.7)	15 (11)	<0.0001
3	61 (10)	55 (11.6)	6 (4.4)	
4	215 (35)	184 (38.7)	31 (22.8)	
5	175 (29)	91 (19)	84 (61.8)	
PRI-MUS (%)				
2	149 (24.3)	136 (28.6)	13 (9.6)	<0.0001
3	60 (9.8)	57 (12)	3 (2.2)	
4	260 (42.5)	211 (44.3)	49 (36)	
5	143 (23.4)	72 (15.1)	71 (52.2)	
ECE MRI (%)				
Present	130 (21.2)	62 (13)	68 (50)	<0.0001
Absent	482 (78.8)	414 (87)	68 (50)	
ECE MUS (%)				
Present	147 (24)	77 (16)	70 (51.5)	<0.0001
Absent	465 (76)	399 (84)	66 (48.5)	

DRE = digital rectal examination; ECE = extracapsular extension; IQR = interquartile range; MRI = magnetic resonance imaging; MUS = microultrasound; OCD = organ-confined disease; PI-RADS = Prostate Imaging Reporting and Data System; PRI-MUS = Prostate Risk Identification Using Micro-Ultrasound; PSA = prostate-specific antigen; PSAD = prostate-specific antigen density.

Table 3 – Uni- and multivariable binary logistic regression analyses predicting side-specific extracapsular extension—MUS based-model

MUS-based model						
Covariate	Univariable analysis			Multivariable analysis		
	OR	95% CI	*p* value	OR	95% CI	*p* value
PSA	1.11	1.07–1.16	<0.0001	1.02	0.95–1.09	0.49
PSAD	20.40	7.35–56.63	<0.0001	7.01	1.37–35.76	**<0.0001**
ISUP grade group						
1	Reference					
2	1.85	0.94–3.65	0.075	0.94	0.44–1.99	0.87
3	3.86	1.94–7.65	<0.0001	1.42	0.65–3.10	0.36
4–5	9.33	4.71–18.46	<0.0001	2.50	1.14–5.51	**0.02**
Maximum % core	1.03	1.02–1.03	<0.0001	1.01	1.00–1.02	**<0.0001**
ECE MUS						
Absent	Reference			Reference		
Present	5.49	3.62–8.32	<0.0001	2.08	1.23–3.50	**0.006**
PRI-MUS						
2	Reference			Reference		
3	0.55	0.15–2.00	0.36	0.56	0.14–2.19	0.41
4–5	4.43	2.41–8.14	<0.0001	1.91	0.92–3.92	0.07
DRE	1.99	1.32–3.00	0.001	1.05	0.63–1.73	0.837

CI = confidence interval; DRE = digital rectal examination; ECE = extracapsular extension; ISUP = International Society of Urological Pathology; MUS = microultrasound; OR = odds ratio; PRI-MUS = Prostate Risk Identification Using Micro-Ultrasound; PSA = prostate-specific antigen; PSAD = prostate-specific antigen density.

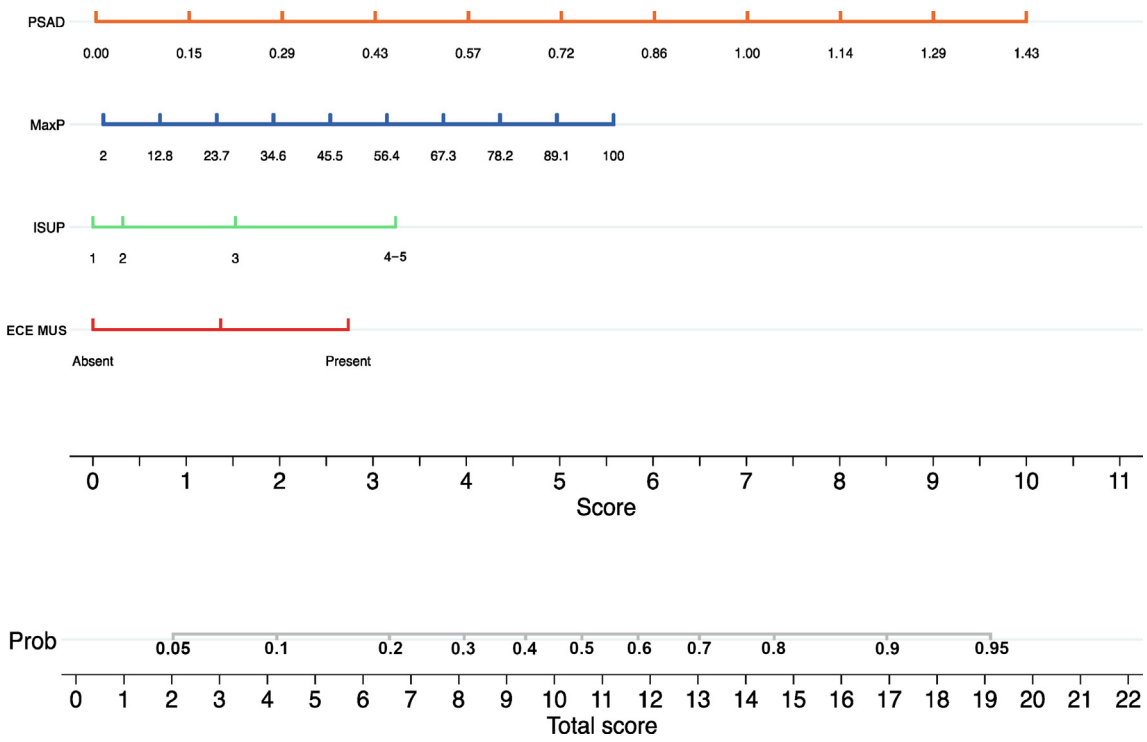

Fig. 2 – Nomogram for the prediction of ECE based on MUS. ECE = extracapsular extension; GGG = Gleason grading group; ISUP = International Society of Urological Pathology; MaxP = maximum percentage of core involvement in the core with the highest GGG; MUS = microultrasound; Prob = probability; PSAD = prostate-specific antigen density.

imaging findings and preoperative clinical parameters. Compared with a model integrating mpMRI and identical clinical parameters, the MUS model resulted in an AUC of 81.4% against the MRI model's 82%. Nonetheless, after internal validation, the AUC was the same for both (80.9%). As presented in the DCA, our nomogram provides a net clinical benefit above a 6.5% threshold by combining PSAD, ISUP GGG, maximum percentage of core involvement in the core with the highest GGG, and presence or absence of ECE on MUS.

Recently, Regis et al [21] found sensitivity, specificity, NPV, and PPV of 87.5%, 80%, 88.9%, and 77.8% for MUS, respectively, in the detection of ECE. Similarly, Fasulo et al [20] reported sensitivity of 72.1%, specificity of 88%, NPV of 80.5%, and PPV of 83.0%. Our outcomes differ mainly for three reasons: first, the PPV of both mpMRI and MUS could have been affected by our lower prevalence of non-OCD compared with the cohort analyzed by Regis et al [21] and Fasulo et al [20] (29.2% vs 44.5% and 43.6%, respectively). Second, 38% of ECE lobes in our cohort were associated with

Table 4 – Uni- and multivariable binary logistic regression analyses predicting side-specific extracapsular extension—MRI-based model

MRI-based model						
Covariate	Univariable analysis			Multivariable analysis		
	OR	95% CI	*p* value	OR	95% CI	*p* value
PSA				1.03	0.97–1.10	0.296
PSAD	11.45	4.86–26.95	<0.0001	7.30	1.14–46.59	**0.035**
ISUP grade group						
1	Reference			Reference		
2	1.85	0.94–3.65	0.075	1.00	0.47–2.10	0.99
3	3.86	1.94–7.65	<0.0001	1.43	0.66–3.08	0.36
4–5	9.33	4.71–18.46	<0.0001	2.78	1.27–6.06	**0.010**
Maximum % core	1.03	1.02–1.03	<0.0001	1.01	1.00–1.02	**<0.0001**
ECE MRI						
Absent	Reference			Reference		
Present	6.67	4.34–10.25	<0.0001	3.17	1.89–5.33	**<0.0001**
PI-RADS						
2	Reference			Reference		
3	0.24	0.75–1.24	0.634	0.96	0.32–2.87	0.94
4–5	1.45	0.87–2.02	<0.0001	1.62	0.82–3.21	0.15

CI = confidence interval; ECE = extracapsular extension; ISUP = International Society of Urological Pathology; MRI = magnetic resonance imaging; OR = odds ratio; PI-RADS = Prostate Imaging Reporting and Data System; PSA = prostate-specific antigen; PSAD = prostate-specific antigen density.

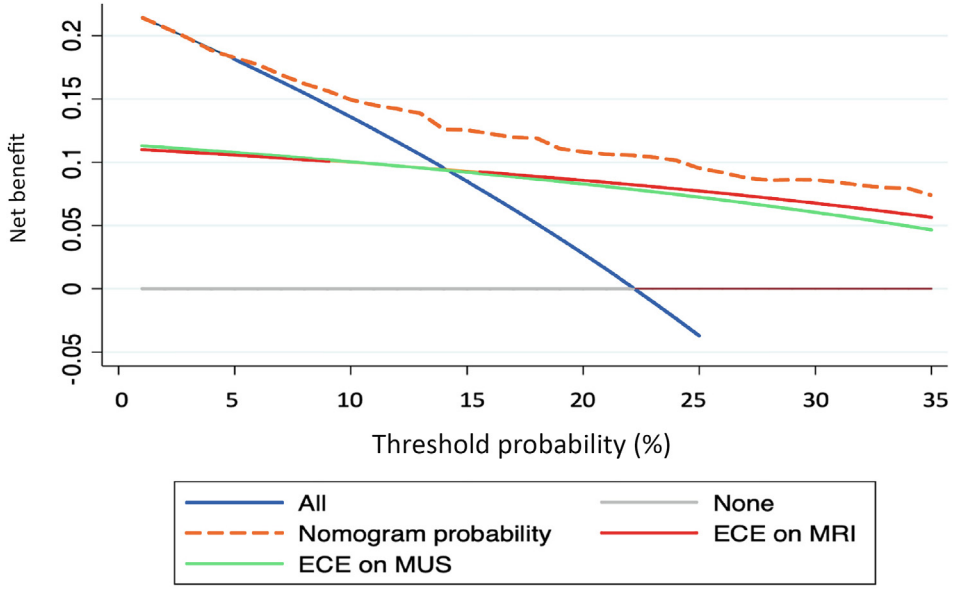

Fig. 3 – Decision curve analysis showing net benefit of using our model based on MUS. ECE = extracapsular extension; MRI = magnetic resonance imaging; MUS = microultrasound.

Table 5 – Agreement in assessing ECE with MUS based on agreement coefficient (AC) and percentage of agreement (PA)

	All	Readers 1 and 2	Readers 1 and 3	Readers 1 and 4
Gwet's AC	0.38 (0.24–0.52)	0.53 (0.33–0.73)	0.33 (0.10–0.56)	0.25 (0.01–0.48)
PA	67.1 (60.7–73.4)	73.1 (63.1–83.1)	64.1 (53.2–74.9)	60.2 (49.1–71.4)

ECE = extracapsular extension; MUS = microultrasound.

abnormal DRE findings, whereas 60% of pT3 prostate cancer patients in the study by Fasulo et al [20] had a palpable disease, with DRE being a significant contributor in their multivariate analysis (odds ratio 3.0). On the contrary, the NNA showed the lowest contribution of DRE (12.1%) for detecting ECE in our patients with no statistical significance in the multivariate model. Lastly, 53% of the lobes with pT3a disease identified in our cohort had either focal or bladder neck invasion. In fact, when the nomogram was applied using established ECE as the primary outcome, the AUC increased to 87%. Those mentioned above, in addition to inter-reader variability, influenced the accuracy of MUS in these different cohorts.

The mpMRI-based model presented here had similar performance to the nomogram published by Martini et al [11], developed at our institution and used in daily practice to guide judgment on grades of nerve preservation during RARP [3]. To provide information regarding the addition of MUS to mpMRI findings and clinicopathologic variables, we integrated nine covariates in the NNA, which showed

higher importance of MUS-related variables than mpMRI-related variables.

Indeed, in our cohort, MUS identified 25 out of the 68 (36%) ECE cases that were overlooked by mpMRI. Interestingly, 12% (3/25) of them corresponded to mpMRI-invisible lesions (PI-RADS 2). This is in concordance with prior reports in the literature, showing up to 26% of cases with clinically significant prostate cancer and negative mpMRI [34,35]. Moreover, all the PI-RADS 3 lesions on mpMRI (4/25) were interpreted as either PRI-MUS 4 or 5 on MUS, a predictor of ECE in our univariate analysis. It is noteworthy that an established or nonfocal ECE was present in 11 out of the 25 cases (44%) missed by mpMRI.

Since adopting MUS in the preoperative setting seems to improve the prediction of ECE, both technologies may therefore be applied in a complimentary manner.

Evaluation of the anterior zone of the prostate can be challenging with MUS, especially in those patients with enlarged prostates and multiple periurethral calcifications. For instance, Chessa et al [36] reported decreased sensitivity and NPV for MUS in detecting clinically significant prostate cancer located in the anterior or transitional zone compared with peripheral zone locations. However, in our cohort of patients, the performance of MUS for the identification of ECE was comparable between the anterior and posterior zone (p = 0.4), as well as for the different locations within the prostate (base and apex; p = 0.65). There were no statistically significant differences in calculated AUCs.

To our knowledge, this is the first described side-specific nomogram integrating MUS and clinicopathologic variables to predict ECE. We have found that the use of this MUS-based model is comparable with that of the mpMRI-based model. Potential advantages of MUS include real-time assessment, lower cost, shorter acquisition time, and avoidance of contrast, making it an attractive preoperative instrument. Moreover, since the urologist performs MUS, it may facilitate the evaluation and interpretation of the test from a surgical perspective.

We acknowledge the limitations of our study, including its sample size, in addition to the that a high percentage of the mpMRI scans were performed at outside facilities and a centralized retrospective review of these readings was not performed. While all MUS scans were done at our institution, the inter-reader agreement was only fair; this could represent a barrier to a wider application. Nonetheless, the AC improved to moderate once the most experienced readers were included in the analysis. On the contrary, the interpretation of MUS may have been biased as the readers were aware of the presence of prostate cancer beforehand. Despite these drawbacks, the integration of MUS as part of a preoperative evaluation produced promising outcomes in creating a nomogram.

5. Conclusions

We have developed a side-specific model to predict ipsilateral ECE based on clinical variables combined with MUS findings. Its performance was comparable with that of a mpMRI-based model using the same clinicopathologic variables (AUC 80.9%). The implementation of this nomogram can be helpful in tailoring nerve-sparing approaches. Nevertheless, external validation of our findings and prospective trials are required to corroborate the results.

***Author contributions*:** Adriana M. Pedraza had full access to all the data in the study and takes responsibility for the integrity of the data and the accuracy of the data analysis.

Study concept and design: Tewari, Pedraza.
Acquisition of data: Parekh, Gupta, Barthe, Pedraza, Pandav.
Analysis and interpretation of data: Joshi, Pedraza.
Drafting of the manuscript: Pedraza, Grauer, Wagaskar, Zuluaga, Gupta, Nasri.
Critical revision of the manuscript for important intellectual content: Tewari, Menon, Gorin, Patel, Pedraza.
Statistical analysis: Joshi, Pedraza.
Obtaining funding: None.
Administrative, technical, or material support: None.
Supervision: Tewari, Pedraza.
Other: None.

Financial disclosures: Adriana M. Pedraza certifies that all conflicts of interest, including specific financial interests and relationships and affiliations relevant to the subject matter or materials discussed in the manuscript (eg, employment/affiliation, grants or funding, consultancies, honoraria, stock ownership or options, expert testimony, royalties, or patents filed, received, or pending), are the following: None.

***Funding/Support and role of the sponsor*:** None.

Appendix A. Supplementary data

Supplementary data to this article can be found online at https://doi.org/10.1016/j.euros.2022.12.005.

References

[1] Moore BM, Savdie R, Pebenito RA, et al. The impact of nerve sparing on incidence and location of positive surgical margins in radical prostatectomy. BJU Int 2012;109:533–8.
[2] Vis AN, van den Bergh RCN, van der Poel HG, et al. Selection of patients for nerve sparing surgery in robot-assisted radical prostatectomy. BJUI Compass 2022;3:6–18.
[3] Martini A, Cumarasamy S, Haines KG, Tewari AK. An updated approach to incremental nerve sparing for robot-assisted radical prostatectomy. BJU Int 2019;124:103–8.
[4] Catalona WJ, Basler JW. Return of erections and urinary continence following nerve sparing radical retropubic prostatectomy. J Urol 1993;150:905–7.
[5] Tewari AK, Srivastava A, Huang MW, et al. Anatomical grades of nerve sparing: a risk-stratified approach to neural-hammock sparing during robot-assisted radical prostatectomy (RARP). BJU Int 2011;108:984–92.
[6] Nyangoh Timoh K, Moszkowicz D, Creze M, et al. The male external urethral sphincter is autonomically innervated. Clin Anat 2021;34:263–71.
[7] Michl U, Tennstedt P, Feldmeier L, et al. Nerve-sparing surgery technique, not the preservation of the neurovascular bundles, leads to improved long-term continence rates after radical prostatectomy. Eur Urol 2016;69:584–97.
[8] Pedraza AM, Pandav K, Menon M, et al. Current strategies to improve erectile function in patients undergoing radical prostatectomy-intraoperative scenario. Urol Oncol 2022;40:79–86.
[9] Eastham JA, Auffenberg GB, Barocas DA, et al. Clinically localized prostate cancer: AUA/ASTRO guideline, Part II: principles of active

surveillance, principles of surgery, and follow-up. J Urol 2022;208:19–25.
[10] Mottet N, van den Bergh RCN, Briers E, et al. EAU-EANM-ESTRO-ESUR-SIOG guidelines on prostate cancer—2020 update. Part 1: screening, diagnosis, and local treatment with curative intent. Eur Urol 2021;79:243–62.
[11] Martini A, Gupta A, Lewis SC, et al. Development and internal validation of a side-specific, multiparametric magnetic resonance imaging-based nomogram for the prediction of extracapsular extension of prostate cancer. BJU Int 2018;122:1025–33.
[12] Giganti F, Coppola A, Ambrosi A, et al. Apparent diffusion coefficient in the evaluation of side-specific extracapsular extension in prostate cancer: development and external validation of a nomogram of clinical use. Urol Oncol 2016;34:291.e9–e17.
[13] Alves JR, Muglia VF, Lucchesi FR, et al. Independent external validation of nomogram to predict extracapsular extension in patients with prostate cancer. Eur Radiol 2020;30:5004–10.
[14] Diamand R, Ploussard G, Roumiguié M, et al. External validation of a multiparametric magnetic resonance imaging–based nomogram for the prediction of extracapsular extension and seminal vesicle invasion in prostate cancer patients undergoing radical prostatectomy. Eur Urol 2021;79:180–5.
[15] Somford DM, Hamoen EH, Fütterer JJ, et al. The predictive value of endorectal 3 tesla multiparametric magnetic resonance imaging for extraprostatic extension in patients with low, intermediate and high risk prostate cancer. J Urol 2013;190:1728–34.
[16] de Rooij M, Hamoen EHJ, Witjes JA, Barentsz JO, Rovers MM. Accuracy of magnetic resonance imaging for local staging of prostate cancer: a diagnostic meta-analysis. Eur Urol 2016;70:233–45.
[17] Laurence Klotz CM. Can high resolution micro-ultrasound replace MRI in the diagnosis of prostate cancer? Eur Urol Focus 2020;6:419–23.
[18] Sountoulides P, Pyrgidis N, Polyzos SA, et al. Micro-ultrasound-guided vs multiparametric magnetic resonance imaging-targeted biopsy in the detection of prostate cancer: a systematic review and meta-analysis. J Urol 2021;205:1254–62.
[19] Kozikowski M, Malewski W, Michalak W, Dobruch J. Clinical utility of MRI in the decision-making process before radical prostatectomy: systematic review and meta-analysis. PLoS One 2019;14:e0210194.
[20] Fasulo V, Buffi NM, Regis F, et al. Use of high-resolution micro-ultrasound to predict extraprostatic extension of prostate cancer prior to surgery: a prospective single-institutional study. World J Urol 2022;40:435–42.
[21] Regis F, Casale P, Persico F, et al. Use of 29-MHz micro-ultrasound for local staging of prostate cancer in patients scheduled for radical prostatectomy: a feasibility study. Eur Urol Open Sci 2020;19:20–3.
[22] Fine SW, Amin MB, Berney DM, et al. A contemporary update on pathology reporting for prostate cancer: Biopsy and radical prostatectomy specimens. Eur Urol 2012;62:20–39.
[23] Samaratunga H, Montironi R, True L, et al. International society of urological pathology (ISUP) consensus conference on handling and staging of radical prostatectomy specimens. Working group 1: specimen handling. Mod Pathol 2011;24:6–15.
[24] Turkbey B, Rosenkrantz AB, Haider MA, et al. Prostate Imaging Reporting and Data System version 2.1: 2019 update of Prostate Imaging Reporting and Data System version 2. Eur Urol 2019;76:340–51.
[25] Luque-Fernandez MA, Redondo-Sánchez D, Maringe C. cvauroc: Command to compute cross-validated area under the curve for ROC analysis after predictive modeling for binary outcomes. Stata J 2019;19:615–25.
[26] Gwet K. Handbook of inter-rater reliability. ed. 4. Gaithersburg, MD: Advanced Analytics; 2014.
[27] Klein D. Implementing a general framework for assessing interrater agreement in Stata. Stata J 2018;18:871–901.
[28] Landis JR, Koch GG. The measurement of observer agreement for categorical data. Biometrics 1977;33:159.
[29] Partin AW, Yoo J, Carter HB, et al. The use of prostate specific antigen, clinical stage and Gleason score to predict pathological stage in men with localized prostate cancer. J Urol 1993;150:110–4.
[30] Nyarangi-Dix J, Wiesenfarth M, Bonekamp D, et al. Combined clinical parameters and multiparametric magnetic resonance imaging for the prediction of extraprostatic disease—a risk model for patient-tailored risk stratification when planning radical prostatectomy. Eur Urol Focus 2020;6:1205–12.
[31] Ohori M, Kattan MW, Koh H, et al. Predicting the presence and side of extracapsular extension: A nomogram for staging prostate cancer. J Urol 2004;171:1844–9.
[32] Soeterik TFW, van Melick HHE, Dijksman LM, et al. Development and external validation of a novel nomogram to predict side-specific extraprostatic extension in patients with prostate cancer undergoing radical prostatectomy. Eur Urol Oncol 2022;5:328–37.
[33] Steuber T, Graefen M, Haese A, et al. Validation of a nomogram for prediction of side specific extracapsular extension at radical prostatectomy. J Urol 2006;175:939–44.
[34] Kuhlmann PK, Chen M, Luu M, et al. Patient- and tumor-level risk factors for MRI-invisible prostate cancer. Prostate Cancer Prostatic Dis 2021;24:794–801.
[35] Rouvière O, Puech P, Renard-Penna R, et al. Use of prostate systematic and targeted biopsy on the basis of multiparametric MRI in biopsy-naive patients (MRI-FIRST): a prospective, multicentre, paired diagnostic study. Lancet Oncol 2019;20:100–9.
[36] Chessa F, Schiavina R, Amelio E, et al. Diagnostic accuracy of the novel 29 MHz micro-ultrasound "exactVuTM" for the detection of clinically significant prostate cancer: a prospective single institutional study. A step forward in the diagnosis of prostate cancer. Arch Ital Urol Androl 2021;93:132–8.